

NUMERICAL INVESTIGATION OF A CASCADED LONGITUDINAL SPACE-CHARGE AMPLIFIER AT THE FERMILAB'S ADVANCED SUPERCONDUCTING TEST ACCELERATOR *

A. Halavanau¹, P. Piot^{1,2}

¹ Department of Physics and Northern Illinois Center for Accelerator & Detector Development, Northern Illinois University, DeKalb, IL 60115, USA

² Accelerator Physics Center, Fermi National Accelerator Laboratory, Batavia, IL 60510, USA

Abstract

In a cascaded longitudinal space-charge amplifier (LSCA), initial density noise in a relativistic e-beam is amplified via the interplay of longitudinal space charge forces and properly located dispersive sections. This type of amplification process was shown to potentially result in large final density modulations [1] compatible with the production of broadband electromagnetic radiation. The technique was recently demonstrated in the optical domain [2]. In this paper we investigate, via numerical simulations, the performances of a cascaded LSCA beamline at the Fermilab's Advanced Superconducting Test Accelerator (ASTA). We especially explore the properties of the produced broadband radiation. Our studies have been conducted with a grid-less three-dimensional space-charge algorithm.

INTRODUCTION

Longitudinal space-charge driven microbunching instabilities arising in bunch compressors (BC) were predicted and observed over the last decade [3–5]. It was recently proposed to employ this microbunching instability mechanism to form attosecond structures in a bunch for the subsequent generation of intense broadband radiation pulses [2, 6]. The experimental setup that enables the generation of space-charge-induced modulation is relatively simple: it consists of focusing sections (e.g. FODO cells) where energy modulations due to the space-charge impedance arise, interspaced with bunch compression chicane. The BCs convert the incoming energy modulation into a density modulation. Several of these (FODO+BC) modules are cascaded so to result in a large final density modulation. Such a modulated beam can be then used to generate coherent radiation at the wavelengths comparable to the modulation period. The purpose of this paper is to explore the possible use of this scheme at the Advance Superconducting Test Accelerator (ASTA) currently under commissioning at Fermilab.

SPACE-CHARGE EFFECTS IN LSCA

When transverse and longitudinal space-charge forces are approximately equal, or longitudinal space-charge force begins to dominate, the particle dynamics within the bunch becomes complicated [7] and microbunching process can be affected by transverse instabilities to a large extent. As

transverse space-charge forces are suppressed by a factor of $1/\gamma^2$, one has to operate at sufficiently large γ to decrease the contribution from transverse space-charge effects. That fact justifies the use of the high energy beamlines (> 300 MeV) (such as ones planned at ASTA facility). Our studies show that the LSCA process is still possible at lower energies, but it requires wider beam sizes to reduce the contribution from the transverse space-charge fields.

The estimated gain per one chicane in LSCA is proportional to space-charge impedance $Z(k, r)$ [8]:

$$G = Ck|R_{56}|\frac{I}{\gamma I_A}\frac{4\pi L_d|Z(k, r)|}{Z_0}e^{-\frac{1}{2}C^2k^2R_{56}^2\sigma_\delta^2}, \quad (1)$$

where R_{56} is the BC longitudinal dispersion, $I_A = 17$ kA is the Alfvén current, L_d is the drift length, σ_δ is the rms fractional energy spread, $C \equiv \langle z\delta \rangle / \sigma_z$ is the chirp, and $Z_0 \equiv 120\pi$ is the free-space impedance.

The exponential term in Eq. 1 induces a high-frequency cut-off of the modulation. Note, that after traveling through a BC, the modulation wavelength will be shortened by a compression factor $(1 + R_{56}C)$. The impedance $Z(k, r)$ is partially determined by the properties of the wakefields inside the BC [8]. Later on, the LSC impedance was shown to mainly cause the effect [1, 6]. The on-axis LSC impedance is given by [9]

$$Z(k) = -i\frac{Z_0}{\pi\gamma\sigma}\frac{\xi_\sigma}{4}e^{\xi_\sigma^2/2}\text{Ei}\left(-\frac{\xi_\sigma^2}{2}\right), \quad (2)$$

and has a maximum at modulations with wave numbers around $k = \gamma/\sigma_\perp$, where σ_\perp is the rms transverse beam size. Thus, by tuning of the betatron function, transverse emittance, beam energy, and compressor parameters, one has some flexibility in selecting the final modulation wavelength.

To characterize the current (density) modulations one can introduce the bunching factor

$$b(\omega) = \frac{1}{N}\left|\sum_n \exp(-i\omega t_n)\right|, \quad (3)$$

where t_n is the temporal coordinate of the n -th macroparticle and N is the total number of particles. The electromagnetic radiation emitted by a bunch of electrons is of the form $\frac{dW}{d\omega d\Omega} = [N + N(N-1)b(\omega)^2]\frac{dW}{d\omega d\Omega}|_1$, where $\frac{dW}{d\omega d\Omega}|_1$ represents the single-electron radiation spectral fluence associated to the considered electromagnetic process.

* This work was supported by the US Department of Energy under contract DE-SC0011831 with Northern Illinois University.

LSCA SIMULATIONS FOR ASTA

The ASTA facility, described elsewhere [10], will soon comprise a 50-MeV injector followed by an accelerator cryomodule capable of boosting the beam energy up to ~ 300 MeV. Eventually, one additional ILC-type cryomodule might be added thereby bringing the final beam energy up to ~ 550 MeV. The injector is capable of producing very low slice transverse emittance around 5×10^{-8} m for 20-pC bunch charge [11]. Although, the LSCA mechanism was previously experimentally demonstrated at low energies [2], a higher-energy beam opens the path to extending the LSCA process to form microstructure with shorter periods (possibility in the extreme ultraviolet regime). This opportunity led us to explore the onset of the LSCA mechanism at the ASTA facility.

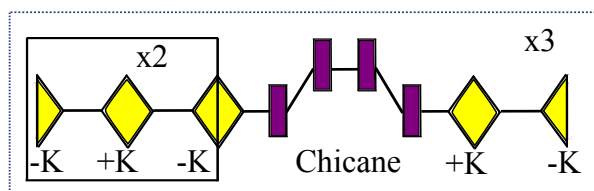


Figure 1: LSCA layout considered in the simulations. The yellow lozenges and purple rectangles respectively represent quadrupole and dipole magnets.

To carry our simulations we employed the tracking program ELEGANT [12] combined with an implementation of the Barnes-Hut algorithm [13]. The code performs full three-dimensional space-charge force calculation and therefore inherits both transverse and longitudinal effects. Further information and test on this “ELEGANT-BH” code can be found in Ref. [15]. The simulations consider the configuration diagrammed in Fig. 1 consisting of three LSCA module each with a lattice composed of three FODO cells with a BC integrated in the last FODO cell (for ease of matching the lattice starts and ends with a half-quadrupole magnet). The total length of 28 m was selected based on the ASTA lattice parameters, although similar simulations can be conducted for shorter or longer LSCA modules. All simulations were done for $N = [0.1..4] \times 10^6$ particles to ensure the convergence and satisfying the statistical limit [14]. Finally, only a small longitudinal slice (taken to be Gaussian in time) was considered; see parameters listed in Tab. 1.

The evolution of the longitudinal phase space distribution appears in Fig. 2. At $\gamma \approx 700$ the instabilities begin to form downstream of the second LSCA module. The shortest microstructures on the longitudinal phase space density are achieved as the LSC-induced modulation has its correlation C satisfying $R_{56} = -1/C$ and finally results in a strongly disrupted longitudinal phase space; see Fig. 2 (bottom right). The microbunches have durations on the order of femtosecond and could in principle be in the attosecond range as investigated in Ref. [6]. Because of the local energy chirp, additional effects related to wakefields and other interactions with radiation [e.g. coherent synchrotron radiation (CSR)]

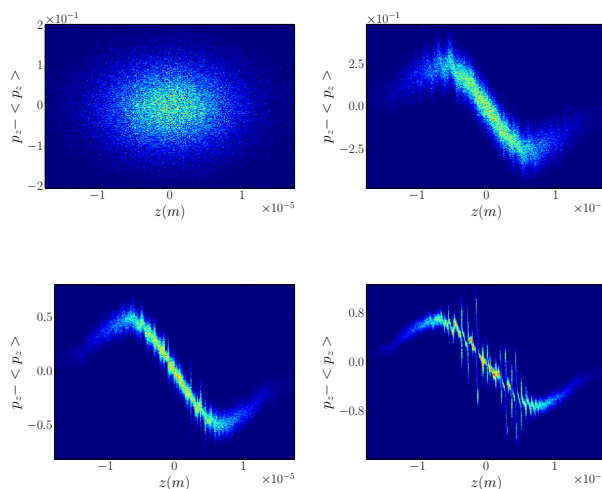


Figure 2: Snapshots of longitudinal-phase space evolution along the cascaded LSCA: initial (Gaussian) bunch before (top left) and after passing through one (top right), two (bottom left) and three (bottom right) LSCA module. The Lorentz factor is $\gamma = 670$.

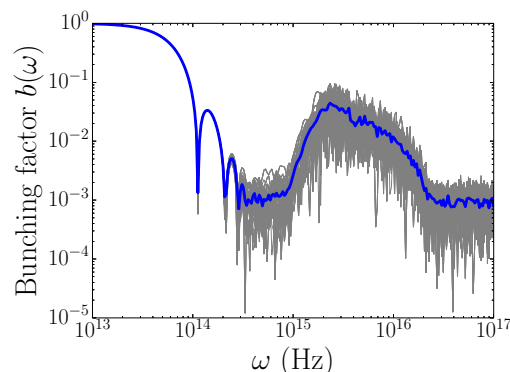


Figure 3: Comparison of averaged bunching factor (blue trace) with bunching factors computed using 100 independent realizations of the initial bunch distributions (gray traces).

Table 1: Beam Parameters Considered for the LSCA Simulations using the Setup of Fig. 1.

Parameter	Value	Units
Spot size, σ	2.2 - 70.4	μm
Charge, Q	20.0	pC
Lorentz factor, γ	50 - 1000	-
Bunch duration, τ	120	fs
Norm. transv. emittance, $\epsilon_{x,y}$	10^{-8}	m
Slice momentum spread, σ_δ	10^{-4}	-
Number of macroparticles, N	$[0.1 - 4] \times 10^6$	-
Total LSCA length, D	28.0	m

should be taken into account. In the present paper we assume the compression process in the chicane is linear (the incoming longitudinal phase space does not have any nonlinear correlations). Cascading more chicanes causes overcompression and microbunching pattern to become highly irregular.

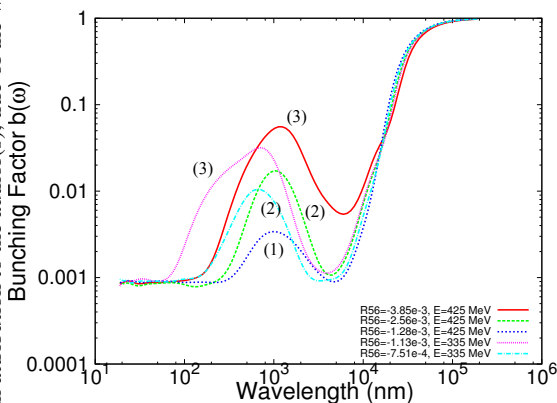


Figure 4: Average bunching factor for various cases of R_{56} and beam energies (see legend). Spline interpolation has been applied. The number in brackets indicates after which LSCA module the bunching factor is evaluated.

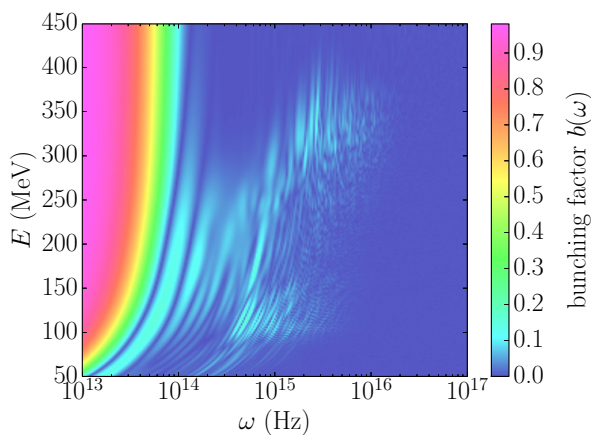


Figure 5: The evolution of the bunching factor $b(\omega)$ as a function of bunch energy.

LSCA is seeded by the initial shot-noise in the beam, therefore to perform a bunching factor analysis, we carried

100 ELEGANT-BH runs for a given lattice setting with different initial random seeds, such to generate independent realizations of initial bunch distributions; see Fig. 3. Figure 4 represents the evolution of the averaged bunching factor for different values of R_{56} and beam energies and demonstrates the flexibility of the LSCA-scheme to produce radiation from the infrared to the vacuum ultraviolet regions. Likewise an energy scan for a fixed value of R_{56} indicates the broad range of operation; see Fig. 5.

CONCLUSIONS AND FUTURE WORK

We presented some preliminary studies of the possible use of a cascaded LSCA scheme to produce femtosecond microstructures in the longitudinal phase space with a period ranging from 200 to 1000 nm. Our study involves beam parameters comparable to the ones achievable at ASTA. Further investigations are needed to refine the designed beamline at ASTA. In addition, further studies will be conducted to explore possible radiation schemes.

REFERENCES

- [1] M. Dohlus, et al., *Proc. SPIE*, 8779 87791T–87791T–15 (2013).
- [2] A. Marinelli, et al., *Phys. Rev. Lett.*, **110** 264802 (2013).
- [3] H. Loos, et al., *SLAC-PUB-13395* (unpublished, 2008).
- [4] P. Piot, et al., *Proc. of EPAC*, 2000.
- [5] M. Borland, *Phys. Rev. ST Accel. Beams*, **11** 030701 (2008).
- [6] M. Dohlus, et al., *Phys. Rev. ST Accel. Beams*, **14** 090702 (2011).
- [7] A. Burov, *Phys. Rev. ST Accel. Beams*, **12** 044202 (2009).
- [8] E.L. Saldin, et al., *Nucl. Inst. Meth. Sec. A*, **483** 516 (2002).
- [9] M. Venturini, *Phys. Rev. ST Accel. Beams*, **11** 034401 (2008).
- [10] E. Harms, et al., *ICFA Beam Dyn. Newslett.*, **64** 133 (2014).
- [11] P. Piot, et al., *Proc. of IPAC'10*, Kyoto, Japan, 4316 (2010).
- [12] M. Borland, *Advanced Photon Source*, LS-287, 2000.
- [13] J. Barnes and P. Hut, *Nature*, **324** 446, Dec 1986.
- [14] C. J. Hirschmugl, et al., *Phys. Rev. A*, **44** 1316 (1991).
- [15] A. Halavanau, and P. Piot, to appear in *Proc. of the IPAC'15*, Richmond, VA, USA (2015).